

DEVELOPMENT OF LOW-Si ALUMINUM CASTING ALLOYS WITH AN IMPROVED THERMAL CONDUCTIVITY

RAZVOJ ALUMINIJEVE LIVARSKE ZLITINE Z MAJHNO VSEBNOSTJO Si IN IZBOLJŠANO TOPLOTNO PREVODNOSTJO

Jesik Shin, Sehyun Ko, Kitae Kim

Production Technology R/D Div., Korea Institute of Industrial Technology, Incheon, South Korea
jsshin@kitech.re.kr

Prejem rokopisa – received: 2012-10-12; sprejem za objavo – accepted for publication: 2013-05-28

To develop an aluminum alloy that can combine a high thermal conductivity with a good castability and anodizability, low Si-containing aluminum alloys, Al-(0.5–1.5)Mg-1Fe-0.5Si and Al-(1.0–1.5)Si-1Fe-1Zn alloys were assessed as potential candidates. The developed alloys exhibited a thermal conductivity of 170–190 % level (160–180 W/(m K)), a fluidity of 60–85 % level, and an equal or higher ultimate tensile strength compared to those of an ADC12 alloy. In each developed alloy system, the thermal conductivity and the strength decreased and increased, respectively, as the content of the major alloying elements, Mg and Si, increased. The fluidity was inversely proportional to the Mg content and directly proportional to the Si content. The Al-(1.0–1.5)Si-1Fe-1Zn alloys showed better thin-wall castability due to their lower surface energy. In the experimental aluminum alloys with a low Si content, the fluidity was mainly dependent on the melt surface energy, the Al dendrite coherency point (DCP), and the first intermetallic crystallization point (FICP), rather than on the solidification interval, latent heat, or the viscosity.

Keywords: alloy design, low-Si aluminum casting alloy, thermal conductivity, castability

Za razvoj aluminijeve zlitine, ki združuje dobro toplotno prevodnost z dobro livnostjo in možnostjo eloksiranja, se predvideva, da sta dobro izhodišče aluminijeve zlitine z majhno vsebnostjo Si, kot sta Al-(0,5–1,5)Mg-1Fe-0,5Si in Al-(1,0–1,5)Si-1Fe-1Zn. Razvite zlitine so pokazale, da je toplotna prevodnost med 170–190 % (160–180 W/(m K)), livnost med 60–85 % in enaka natezna trdnost, kot jo ima primerjalna zlitina ADC12. V vsakem razvitem sistemu je toplotna prevodnost naraščala in trdnost padala, ko je naraščala vsebnost glavnih legirnih elementov Mg in Si. Tekočnost je bila obratno sorazmerna z vsebnostjo Mg in sorazmerna z vsebnostjo Si. Zlitina Al-(1,0–1,5)Si-1Fe-1Zn je pokazala boljšo livno sposobnost pri tankih stenah zaradi manjše površinske energije. Pri preizkusnih aluminijevih zlitinah z majhno vsebnostjo Si je bila tekočnost predvsem odvisna od površinske energije taline, koherentne točke Al-dendritov (DCP) in prve točke strjevanja (FICP) intermetalne zlitine in manj od intervala strjevanja, latentne toplote ali viskoznosti.

Ključne besede: oblikovanje zlitine, aluminijeva livna zlitina z majhno vsebnostjo Si, toplotna prevodnost, livna sposobnost

1 INTRODUCTION

As the amount of heat that needs to be removed from electric devices such as LED lighting increases rapidly with the tendency towards higher outputs, the development of heat-dissipating components has recently become a subject of special interest. Aluminum, the most common heat-sink material, has inherent disadvantages that need to be overcome. Although high-purity aluminum possesses excellent thermal conductivity, it is extremely difficult to diecast; thus, alloying elements must be added, despite the thermal conductivity loss that occurs as a result of adding these alloying elements. The ADC12 alloy, a commercial Al–Si-based aluminum alloy, has been the most common aluminum alloy for heat-sinks. A heat-sink with a three-dimensional complex shape that is favorable to heat dissipation can be fabricated in a net shape, with a high productivity and without the cost penalty that comes with using a high-pressure diecasting process, like with the ADC12 alloy. However, a low thermal conductivity below 100 W/(m K) and the poor anodizing characteristics of the ADC12

alloy, caused by its high Si content, are becoming serious problems with the increasing power requirements of electric devices. Other commercial aluminum alloys are also difficult to diecast or exhibit a conductivity that is too low for them to be used as heat-dissipating components for high-power electric devices.^{1–4}

Therefore, the aim of this study was to develop a novel, low-Si-containing anodizable aluminum alloy that possesses both a good thermal conductivity and castability. To achieve this goal, the elements known to have advantages in improving castability, strengthening the matrix, and preventing die sticking as well as to have a minimal effect on the resistivity increment of aluminum, such as Mg, Si, Zn, and Fe, were chosen and alloyed. The amounts of the total alloying elements and Si were kept between mass fractions 2 % and 3.5 %, and below 1.5 %, respectively. The thermal conductivity, fluidity, and mechanical strength of the newly designed Al-*x*Mg-1Fe-0.5Si and Al-*x*Si-1Fe-1Zn alloys were investigated as functions of the Mg and Si content and compared to those of the ADC12 alloy.

2 EXPERIMENTAL

2.1 Alloy design

To achieve the combination of a high thermal conductivity and good castability and anodizability, two low-Si quaternary aluminum alloys were designed as follows. First, in terms of the effects of the alloying elements on the electrical resistivity,⁵ energy release for solidification,⁶ and viscosity^{5,7} of aluminum, as shown in **Table 1**, Mg and Si were chosen as the major alloying elements. The energy release for solidification was obtained by summing the latent heat and the superheating energy calculated for a superheat of 100 °C using the specific heat of each element according to the simple mixture rule. A low electrical resistivity and viscosity, and a high-energy release for the solidification are preferred because the decreasing electrical resistivity tends to increase the thermal conductivity, while increasing the energy release for solidification and decreasing the viscosity, both of which tend to increase the requirements for good castability, such as melt fluidity. The elements marked with an asterisk (*) in **Table 1** are those that are considered favorable to thermal conductivity and castability. Thus, it can be seen that only two elements,

Mg and Si, meet all the required conditions. Secondly, Fe was included to prevent mold-sticking problems. Lastly, Si and Zn were utilized as supplementary alloying elements, as described below.

In **Table 2**, the constituent elements of the two low-Si quaternary aluminum alloy systems, Al-xMg-Fe-Si (Alloy 1 series) and Al-xSi-Fe-Zn (Alloy 2 series), and their chemical compositions are summarized. The total amounts of alloying elements were kept between mass fractions 2 % and 3.5 % to achieve a good balance of thermal conductivity and castability. The amounts of Mg and Si were varied from 0.5 % to 1.5 % in order to systematically investigate the effects of these major alloying elements on the thermal conductivity and castability. If the alloying levels are too high or too low, the thermal conductivity and castability may deteriorate, respectively. Because the Si particles decrease the anodizability, the level of Si in particular was kept below 1.5 %, which is the maximum amount of Si in commercial wrought Al alloys known to have good anodizability. The amount of Fe was 1 %, the same as in the ADC12 alloy. In the Al-xMg-Fe-Si alloys, 0.5 % Si was added as a supplementary element to effectively increase the energy

Table 1: Effects of alloying elements on electrical resistivity,⁵ energy release for solidification,⁶ and viscosity of aluminum^{5,7} (calculation was made for ΔT of 100 °C)

Tabela 1: Vpliv legirnih elementov na električno upornost,⁵ energijo, sproščeno pri strjevanju,⁶ in viskoznost aluminija^{5,7} (izračun je bil izdelan za ΔT 100 °C)

Element	Resistivity			Energy release for solidification			Viscosity variation of Al with alloying
	Maximum solubility in Al (w/%)	Resistivity increment of Al per w/‰ (μΩ cm)		Latent heat, H of pure elements (kJ/kg)	Specific heat, c' of pure elements (kJ/kg)	H + c'ΔT increment of Al per w/‰ (kJ/kg)	
		In solution	Out of solution				
Cr	0.77	4.00	0.180	402	0.66	-0.3	(+)
Cu	5.65	*0.34	0.030	205	0.45	-2.5	(+)
Fe	*0.05	2.56	0.058	272	0.78	-1.5	(+)
Li	4.00	3.31	0.680	422	4.46	*3.7	
Mg	14.90	*0.54	0.220	362	1.34	*0.0	*(-)
Mn	1.82	2.94	0.340	268	0.70	-1.6	(+)
Ni	*0.05	*0.81	0.061	292	0.56	-1.5	(+)
Si	1.65	*1.02	0.088	1804	0.93	*14.0	*(-)
Ti	1.00	2.88	0.120	366	0.68	-0.6	(+)
V	0.50	3.58	0.280	329	0.62	-1.1	
Zn	82.80	*0.09	0.023	111	0.48	-3.4	*(0)
Zr	0.28	1.74	0.044	212	0.37	-2.5	

Table 2: Chemical composition in mass fractions (w/%) of the developed low-Si aluminum alloys Al-xMg-Fe-Si (alloy 1 series) and Al-xSi-Fe-Zn (alloy 2 series)

Tabela 2: Kemijska sestava v masnih deležih (w/%) razvitih aluminijevih zlitin z majhno vsebnostjo Si, Al-xMg-Fe-Si (zlitina 1. serije) in Al-xSi-Fe-Zn (zlitina 2. serije)

Alloy	Major Element		Anti-die-sticking element	Supplementary element		Base element	Thermal conductivity (W/(m K))	
	Mg	Si	Fe	Zn	Si	Al		
1	1-1	0.5	-	1.0	-	0.5	98.0	186
	1-2	1.0	-	1.0	-	0.5	97.5	175
	1-3	1.5	-	1.0	-	0.5	97.0	160
2	2-1	-	1.0	1.0	1.0	-	97.0	171
	2-2	-	1.2	1.0	1.0	-	96.8	163
	2-3	-	1.5	1.0	1.0	-	96.5	153

release for solidification. Because Si has been reported to be less effective in strengthening the Al matrix than Mg,⁵ 1 % Zn was added as a supplementary element in the Al-xSi-Fe-Zn alloys. Although heat-sinks are not structural components that need a very high strength, proper strength is imperative in order to eject the castings from molds safely. Moreover, Zn has the lowest resistivity increment, as shown in **Table 1**. The thermal conductivities of the alloys were calculated by a simple rule-of-mixture and the Wiedemann-Franz law using the data of **Table 1** in order to predict the effects of the elements on the resistivity of Al.

2.2 Evaluation and analyses

The fluidity test was conducted using a ceramic-coated steel mold with multiple channels on a low-pressure casting machine under an inert-gas atmosphere in order to prevent melt oxidation. **Figure 1a** shows the parting plane of the metal mold for the fluidity test. The flow channels were 100 mm long and open to the air at the end, and their diameters were (8, 4, 2, and 1) mm. **Figure 1b** shows the fluidity test casting after solidification. The average flow lengths for each channel diameter were taken as the fluidity values, and 10 experiments were performed to confirm the reproducibility. To evaluate the fluidity only as a function of alloy composition, the mold temperature, the superheat temperature, and the

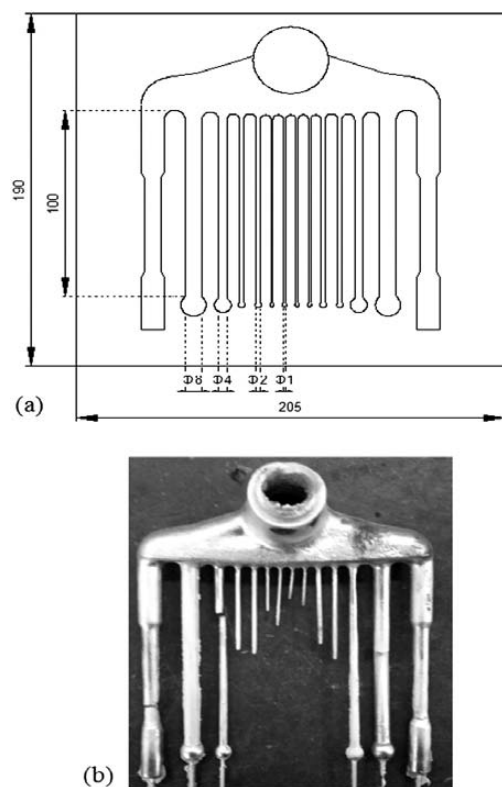


Figure 1: a) Parting plane of the metal mold for fluidity test and b) fluidity test casting

Slika 1: a) Načrt debeline delov pri preizkusu tekočnosti in b) ulitek po preizkusu tekočnosti

pressure during pouring were kept constant: 190 °C, 100 °C, and 15 kPa, respectively. The melting points of the alloys were determined by a thermal analyzer TG/DTA, model SDT Q600, applying a heating rate of 10 °C/min up to 700 °C in an Ar atmosphere (flow rate: 0.1 L/min).

The thermal conductivities of the alloys were drawn from their electrical resistivities as measured by an eddy-current technique, utilizing the Wiedemann-Franz law to determine the relation between the electrical resistivity and the thermal conductivity. The tensile strength evaluation was carried out according to ASTM B 557M using specimens taken from a Y-block casting with dimensions of 200 mm × 150 mm × 25 mm. The ADC12 alloy (Al-10 % Si-2.5 % Cu-1 % Fe-0.2 % Mg) was used as a comparative material for the properties evaluation of the developed alloys.

Thermophysical modeling using the commercial software JMatPro 5.0 was performed to obtain the thermophysical properties relating to castability and the phase-equilibria information. For microstructural analysis, including phase characterization, the cross-sections of the fluidity test channels were examined using a field-emission scanning electron microscope (FESEM), model FEI Quanta 200F, equipped with an energy-dispersive spectroscopy (EDS) probe. To understand the solidification paths, cooling curve analyses (CCA) were carried out based on the two-thermocouple method.^{8,9} Two K-type thermocouples, one at the center (TC) of the graphite mold and one near the wall (TW), were positioned to record the solidification history, as shown in **Figure 2**. Then the graphite mold was dipped into the melt for about 30 s to fill it up and allow its temperature to equilibrate with the melt temperature. According to Farahany's method,⁸ the temperature at which the first maximum difference between the thermocouples TC and TW occurred is regarded as the dendrite coherency point (DCP).

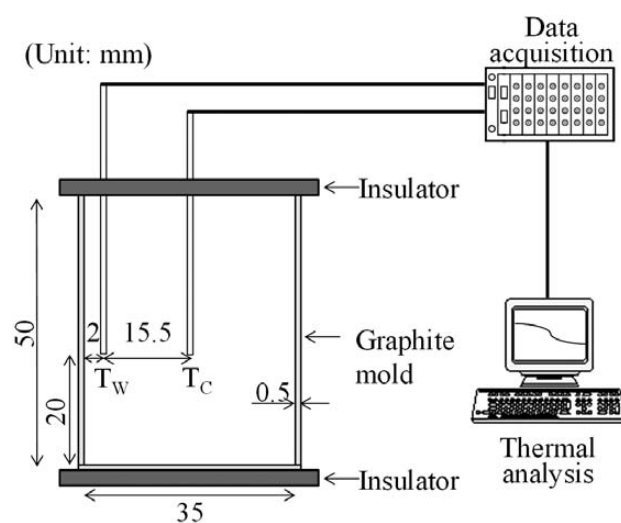


Figure 2: Cooling-curve analysis, set-up with a graphite mold and two K-type thermocouples

Slika 2: Sestav za analizo ohlajevalnih krivulj z grafitno kokilo in dvema termoelementoma vrste K

3 RESULTS AND DISCUSSION

The measured thermal conductivity, fluidity, and ultimate tensile strength of the developed Al-xMg-1Fe-0.5Si and Al-xSi-1Fe-1Zn alloys were compared to those of the ADC12 alloy and the results are summarized in **Figure 3**. The developed alloys showed a higher thermal conductivity of 160–180 W/(m K), which is approximately 70–90 % higher than that of the ADC12 alloy, as shown in **Figure 3a**. The thermal conductivity of the alloys decreased with the increment of Mg and Si, the major alloying elements. The difference in the thermal conductivity between the two alloy systems was fairly insignificant. The average flow lengths for the diameter channels 1 mm and 2 mm are summarized in **Figure 3b**. The channels larger than 2 mm in diameter were completely filled for both alloy melts. The fluidity of the developed alloys reached 60–85 % that of the ADC12 alloy, which was obtained by averaging the flow length for the diameter channels 2 mm. It was found that the fluidity of the Al-xMg-1Fe-0.5Si alloys decreased with increasing Mg content, whereas that of the Al-xSi-1Fe-1Zn alloys increased with increasing Si content. Interestingly, the opposite tendency was observed between the two alloy systems with a changing channel diameter, i.e., for the diameter channels 2 mm, the

Al-xMg-1Fe-0.5Si alloys showed a higher fluidity than the Al-xSi-1Fe-1Zn alloys, but this tendency was reversed for the diameter channels 1 mm. The tensile strength of the two alloy systems increased with increasing Mg and Si contents, reaching an equal or higher tensile strength than the ADC12 alloy, as shown in **Figure 3c**. The strength of the Al-xMg-1Fe-0.5Si alloys was higher than that of the Al-xSi-1Fe-1Zn alloys.

To understand the fluidity behavior, which is more complex than understanding the thermal conductivity or strength, important thermophysical properties relating to the castability were calculated by JMatPro software and are summarized in **Figure 4**. **Figure 4a** shows the variation of the energy release for solidification as a function of the contents of Mg and Si. From a higher perspective, the two alloy systems showed similar levels of energy release for solidification. However, looking within each alloy system, the energy release of solidification for the Al-xMg-1Fe-0.5Si alloys did not change until reaching a mass fraction 1.0 % Mg and then it decreased. Considering that Mg is an element with almost the same energy release for solidification as Al, the solidification path and crystallization phases seemed to change as the Mg content increased from 1.0 % to 1.5 %. In the Al-xSi-1Fe-1Zn alloys, the energy release for solidification increased in proportion to the amount of Si. To summa-

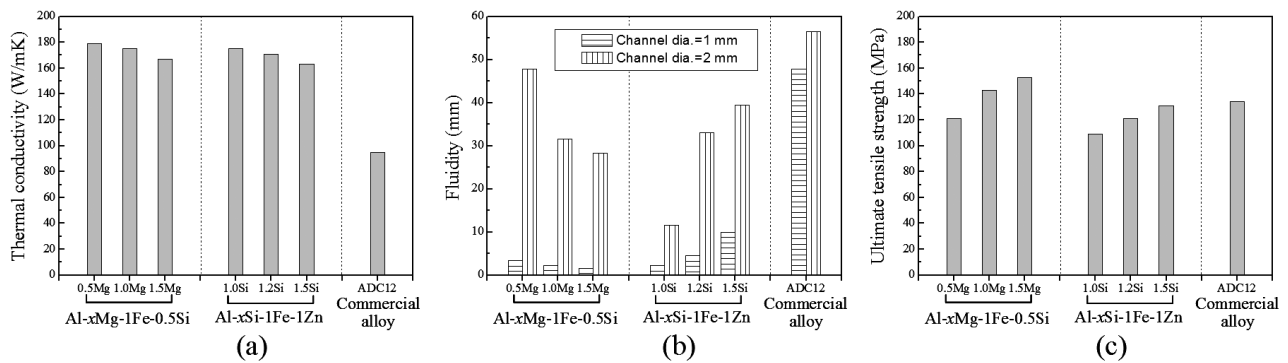


Figure 3: Measured: a) thermal conductivity, b) fluidity and c) ultimate tensile strength of Al-(0.5–1.5)Mg-1Fe-0.5Si and Al-(1.0–1.5)Si-1Fe-1Zn alloys

Slika 3: Izmerjena: a) toplotna prevodnost, b) tekočnost in c) natezna trdnost zlitin Al-(0,5–1,5)Mg-1Fe-0,5Si in Al-(1,0–1,5)Si-1Fe-1Zn

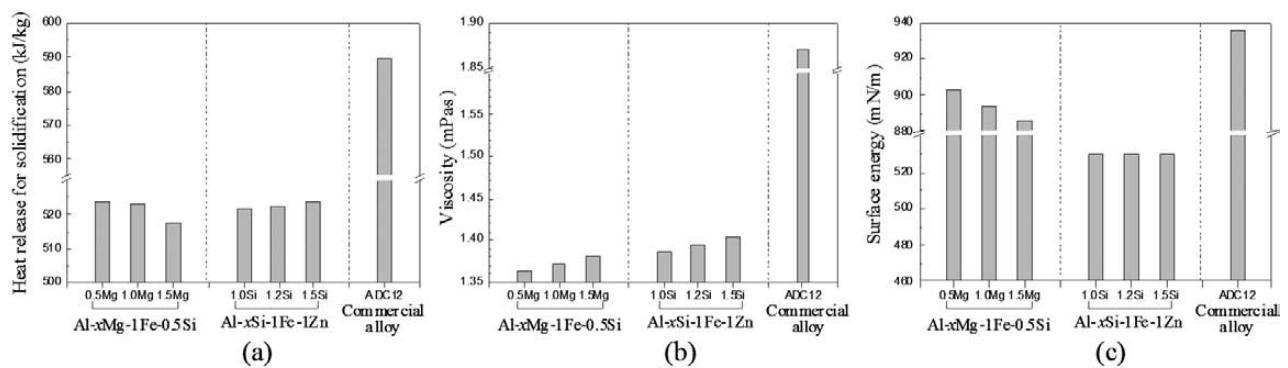


Figure 4: a) Heat release for solidification, b) viscosity and c) surface energy of Al-(0.5–1.5)Mg-1Fe-0.5Si and Al-(1.0–1.5)Si-1Fe-1Zn alloys calculated by JMatPro

Slika 4: a) Sproščanje toplote pri strjevanju, b) viskoznost in c) površinska energija zlitin Al-(0,5–1,5)Mg-1Fe-0,5Si in Al-(1,0–1,5)Si-1Fe-1Zn, izračunana z JMatPro

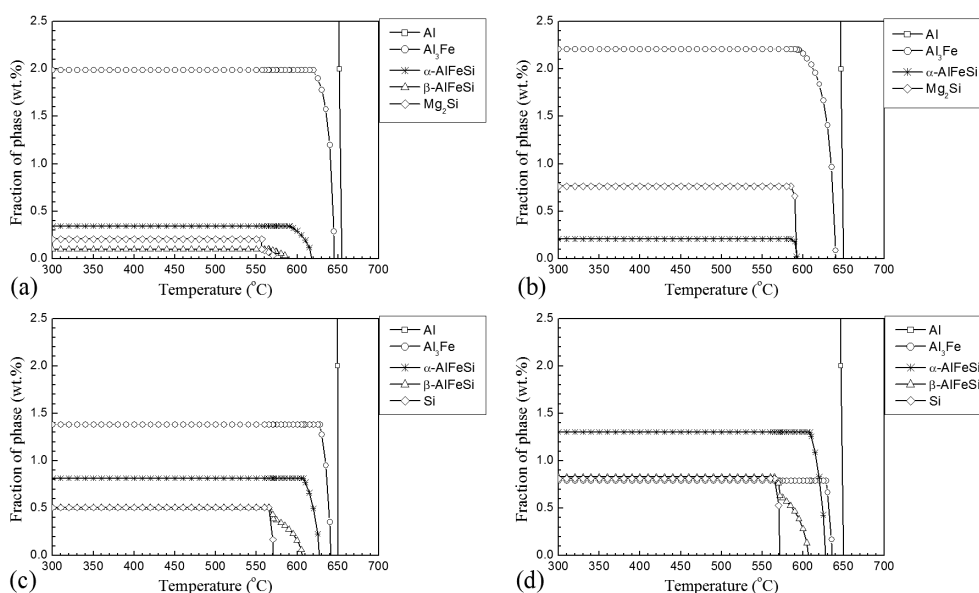


Figure 5: Phase equilibria calculated by JMatPro: a) Al-0.5Mg-1Fe-0.5Si, b) Al-1.5Mg-1Fe-0.5Si, c) Al-1.0Si-1Fe-1Zn and d) Al-1.5Si-1Fe-1Zn alloys

Slika 5: Fazna ravnotežja v zlitinah, izračunana z JMatPro: a) Al-0,5Mg-1Fe-0,5Si, b) Al-1,5Mg-1Fe-0,5Si, c) Al-1,0Si-1Fe-1Zn in d) Al-1,5Si-1Fe-1Zn

rise, the variation of energy release for the solidification coincided relatively well with the fluidity behavior, but the variation in the quantity of energy release for solidification was too small to fully explain the fluidity variation. **Figure 4b** shows the viscosity of the developed alloys calculated under the same superheat conditions. For both alloy systems, the viscosity increased in proportion to the amount of Mg and Si. It seemed that in this investigation, the viscosity did not have a significant effect on the fluidity of these experimental alloys. For reference, the reason why the viscosity decreased with increasing Mg and Si content in the work of other researchers^{5,7} was that the viscosity was obtained not for a constant superheat condition but for a constant pouring-temperature condition, i.e., the variation of the liquidus temperature of the various alloy compositions was not considered. On the other hand, it is notable that the difference in the surface energy between the two alloy systems was significant, as shown in **Figure 4c**. It seemed that the superior fluidity for the small diameter channel of the Al-*x*Si-1Fe-1Zn alloys was because of the lower backpressure caused by a lower surface energy. It is apparent that the Al-*x*Si-1Fe-1Zn alloys showed a similar energy release during the solidification and even a higher viscosity, but their surface energies were nearly half those of the Al-*x*Mg-1Fe-0.5Si alloys. Actually, in this fluidity test experiment, which used a low-pressure casting machine, the backpressure in the diameter channels 1 mm calculated by the capillary effect amounted to approximately 80 % of the applied pouring pressure.

Because the solidification range and secondary phases also have an influence on the fluidity of alloy melts,^{10–15} the phase-equilibria calculations were carried out prior to the microstructural examination. **Figure 5** shows the phase equilibria during solidification calcu-

lated by the Scheil equation (the nonequilibrium lever rule) using JMatPro. The Al-*x*Mg-1Fe-0.5Si alloys were typified by the fact that the amount of Al₃Fe phase, which has been reported to have a plate shape,¹¹ increased with increasing Mg content, whereas the solidification range decreased significantly as a result of the change of the quaternary eutectic point. In the Al-*x*Si-1Fe-1Zn alloys, the liquidus temperature decreased slightly with Si content but the quaternary eutectic point did not change, resulting in a slight decrease in the solidification range. In addition, the amount of Al₃Fe phase, which was formed by the first monovariant eutectic reaction, decreased with increasing Si content. At 1.5 % Si, the amount of the Al₃Fe phase became less than the amount of the α -AlFeSi phase, which was formed by the subsequent monovariant eutectic reaction. From these calculated solidification characteristics, it is thought that the Al₃Fe phase played a role in lessening the fluidity of the Al-*x*Mg-1Fe-0.5Si and Al-*x*Si-1Fe-1Zn alloys. The decrease in the solidification range in the Al-*x*Mg-1Fe-0.5Si alloys might also have provoked the negative effect of the Al₃Fe phase on the fluidity, which is different from the general tendency of a narrower solidification range improving the melt fluidity.¹⁰ In other words, the decrease in the solidification range resulted in an increase in the residual liquid fraction at the stage when the Al₃Fe phase started to form. As the Mg increased from 0.5 % to 1.5 %, the residual liquid fraction increased from 50 % to 60 %, thus enlarging the Al₃Fe phase with its large aspect ratio and finally obstructing the melt flow.

To investigate the actual nonequilibrium solidification characteristics, cooling-curve analyses and microscopic tests were carried out. In **Figure 6**, the cooling-curve analyses results, which consist of cooling curves,

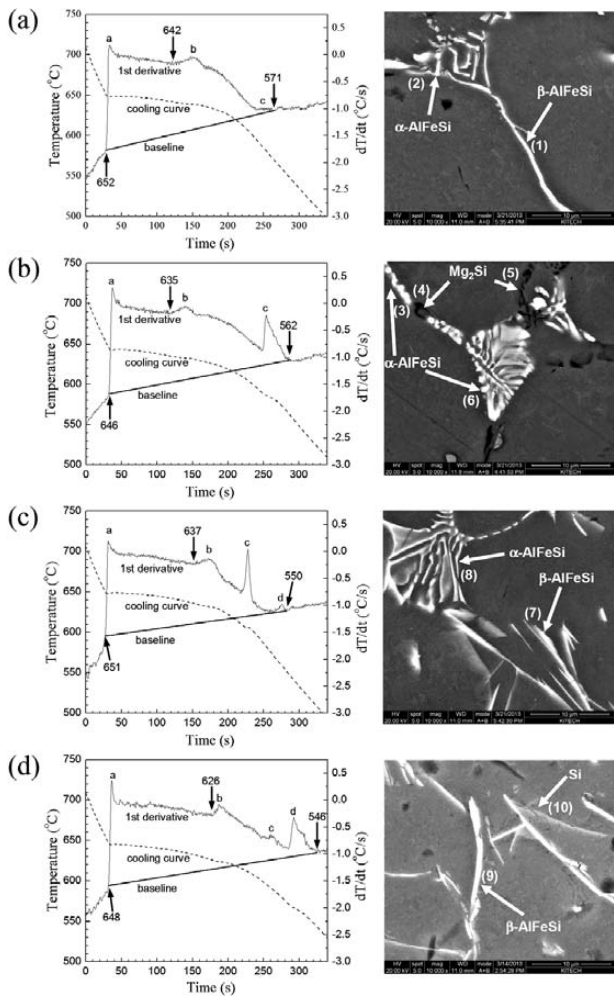


Figure 6: Cooling-curve analysis results and SEM (BSE) microstructural images in as-cast state: a) Al-0.5Mg-1Fe-0.5Si, b) Al-1.5Mg-1Fe-0.5Si, c) Al-1.0Si-1Fe-1Zn and d) Al-1.5Si-1Fe-1Zn alloys
Slika 6: Rezultati analize ohlajevalnih krivulj in SEM- (BSE)-posnetki mikrostruktur zlitin v litem stanju: a) Al-0,5Mg-1Fe-0,5Si, b) Al-1,5Mg-1Fe-0,5Si, c) Al-1,0Si-1Fe-1Zn in d) Al-1,5Si-1Fe-1Zn

their first derivatives, and baselines, and the scanning electron microscopy images with backscattered electrons [SEM(BSE)] in the as-cast state are shown. In the Al-xMg-1Fe-0.5Si alloys (Figures 6a and 6b), three thermal events are observed in the first-derivative curves. At the onset of solidification of any phase, the first derivative increases in value and decreases upon the completion of solidification.⁸ It appears that the peaks labeled (a), (b), and (c) correspond to the crystallization of primary Al dendrites, the formation of secondary phases at the inter-dendritic regions between the secondary dendrite arms, and the final eutectic solidification reaction, respectively. From the results of the combined SEM (BSE) and EDS analyses, which are shown in Table 3, it was verified that in the Al-0.5Mg-1Fe-0.5Si alloy (Figure 6a) the plate-shaped particle (1) between the secondary dendrite arms was a β -AlFeSi phase and the irregular-shaped particle (2) at the final solidification regions was an α -AlFeSi phase. According to Rosefort et

al.,¹⁶ α - and β -AlFeSi phases in as-cast aluminum alloys can be identified with the help of SEM-EDS, i.e., the phase with the plate-like structure at high Si(wt%)/Fe(wt%) ratios above approximately 0.4 is a β -AlFeSi phase and the phase with the Chinese-script-structure at low Si(wt%)/Fe(wt%) ratios is an α -AlFeSi phase. In the high-Mg-containing Al-1.5Mg-1Fe-0.5Si alloy (Figure 6b), a dotted bright particle (3) and a dark particle (4) were observed at the inter-dendritic regions between the secondary dendrite arms. These dotted bright and dark particles proved to be α -AlFeSi and Mg₂Si phases, respectively. The Mg₂Si phase was also observed at the final solidification regions [particle (5)]. It is likely that the peak (c) on the first derivative curve of Figure 6b, which is larger than that of Figure 6a, was related to a larger latent-heat evolution due to Mg₂Si phase crystallization. In the Al-xSi-1Fe-1Zn alloys, four thermal events were observed on the first-derivative curves, as shown in Figures 6c and 6d, and it was determined that the peaks (a), (b), (c), and (d) corresponded to the crystallization of primary Al dendrites, the β -AlFeSi phase at the inter-dendritic regions between secondary dendrite arms, and α -AlFeSi and Si phases at the final solidification regions, respectively. The results indicate that in the Al-1Si-1Fe-1Zn alloys (Figure 6c) the peak (c) tended to be relatively larger than the peak (d). The reverse findings in the Al-1.5Si-1Fe-1Zn alloys (Figure 6d) were attributed to the microstructural differences in the final solidification regions with Si content. That is, in a low-Si-containing Al-1Si-1Fe-1Zn alloy, an α -AlFeSi phase was mostly observed in the final solidification regions, but in a high-Si-containing Al-1.5Si-1Fe-1Zn alloy, the Si and β -AlFeSi phases prevailed.

Table 3: EDS analysis of the compositions of the particles (1)–(10) marked in Figure 6

Tabela 3: EDS-analiza sestave delcev (1)–(10), označenih na sliki 6

Point	Mg		Si		Fe		Zn		Al
	wt%	at%	wt%	at%	wt%	at%	wt%	at%	
(1)	0.75	0.88	5.03	5.11	10.46	5.35	–	–	bal.
(2)	0.43	0.51	1.55	1.58	10.97	5.62	–	–	bal.
(3)	1.82	2.16	1.12	1.15	12.86	6.65	–	–	bal.
(4)	6.79	7.54	6.42	6.17	1.01	0.49	–	–	bal.
(5)	8.05	8.92	4.63	4.44	1.17	0.56	–	–	bal.
(6)	1.93	2.32	1.38	1.44	14.96	7.82	–	–	bal.
(7)	–	–	7.42	7.56	10.54	5.40	0.16	0.19	bal.
(8)	–	–	4.95	5.16	12.92	6.78	1.78	0.80	bal.
(9)	–	–	9.45	9.71	9.91	5.12	1.71	0.76	bal.
(10)	–	–	17.15	17.11	3.02	1.51	2.46	1.05	bal.

Unlike the calculated phase equilibria during solidification, shown in Figure 5, an Al₃Fe phase (or the metastable Al₆Fe phase) was not observed in the metallographic inspection for any of the Al-xMg-1Fe-0.5Si and Al-xSi-1Fe-1Zn alloys, as shown in Figure 6. Moreover, it is interesting to note that β -AlFeSi, a low-temperature-stable phase, crystallized earlier than α -AlFeSi, a high-temperature-stable phase, at the inter-dendritic

regions between the secondary dendrite arms. Except for the high-Mg-containing alloy (the Al-1.5Mg-1Fe-0.5Si alloy), the α -AlFeSi phase was observed only in the final solidification regions. These solidification characteristics could be attributed to the segregation behavior of the solute atoms, particularly Si. That is because the cooling rate was high and the solidification occurred as a fine, mushy type, the Si atoms ejected into the interdendritic liquid had little chance of diffusing out to a residual liquid reservoir because of the limited time and space. As a result, the β -AlFeSi phase with a high Si/Fe ratio was crystallized at interdendritic regions between the secondary dendrite arms rather than the α -AlFeSi. Thus, for the final solidification regions, which had relatively longer solidification times and lower Si concentrations than the inter-dendritic regions, an α -AlFeSi phase could crystallize. These are consistent with Darvishi's experimental results¹³ regarding the presence of silicon-substituted Al₃Fe and Al₆Fe phases with α - and β -AlFeSi phases and with Dutta's simulation results,¹⁷ which show that the increase in the cooling rate increased the Si/Fe ratio in the eutectic liquid. In the high-Mg-containing alloy (Al-1.5Mg-1Fe-0.5Si alloy) it is likely that the consumption of Si atoms due to the formation of a Mg₂Si phase enabled the α -AlFeSi phase to crystallize, even at the inter-dendritic regions between the secondary dendrite arms under the same cooling conditions. Hosseini-far et al.¹⁸ reported a similar phase selection example in a 6xxx Al alloy: the addition of La resulted in the formation of a La(Al,Si)₂ phase and a decrease of the

Si/Fe ratio in the eutectic liquid, favoring the crystallization of an α -AlFeSi phase rather than a β -AlFeSi phase.

The characteristic solidification parameters, including the solidification range, were calculated from the cooling and first-derivative curves and the results are summarized in **Table 4**. However, it seems that the Al-*x*Mg-1Fe-0.5Si and Al-*x*Si-1Fe-1Zn alloys did not follow the general relation between the solidification range and the fluidity length of the alloy very well, in which the fluidity length is inversely proportional to the solidification range. DCP and the first intermetallic crystallization point (FICP) also did not seem to show a direct relation with the fluidity length. The onset temperatures for the (b) peaks in **Figure 6**, which were determined by the tangential line method, were used as the FICP.

Table 4: Characteristic solidification parameters for Al-*x*Mg-Fe-Si (alloy 1 series) and Al-*x*Si-Fe-Zn (alloy 2 series) alloys

Tabela 4: Značilni parametri strjevanja za Al-*x*Mg-Fe-Si (zlitina 1. serije) in Al-*x*Si-Fe-Zn (zlitina 2. serije)

Alloy	Start of solidification (°C)	End of solidification (°C)	Solidification range (°C)	FICP (°C)	DCP (°C)
1	1-1	652	571	81	642
	1-2	649	558	91	637
	1-3	646	562	84	635
2	2-1	651	550	101	637
	2-2	648	550	98	630
	2-3	648	546	102	626

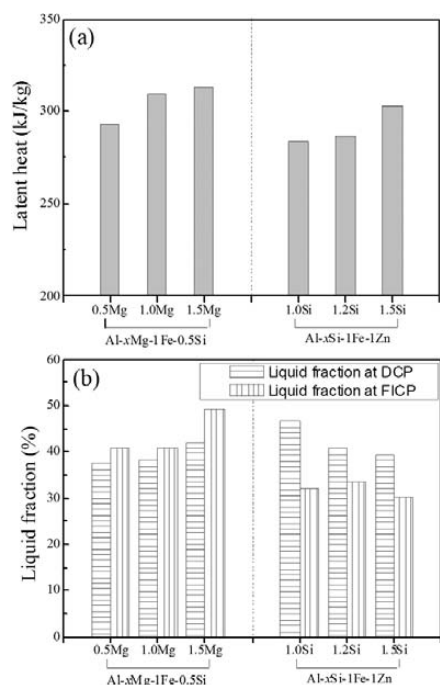


Figure 7: a) Latent heat and b) liquid fraction at DCP and FICP of Al-(0.5–1.5)Mg-1Fe-0.5Si and Al-(1.0–1.5)Si-1Fe-1Zn alloys, which were obtained from a cooling-curve analysis

Slika 7: a) Latentna toplota in b) delež taline pri DCP- in FICP-zlitin Al-(0,5–1,5)Mg-1Fe-0,5Si in Al-(1,0–1,5)Si-1Fe-1Zn, dobljeni iz analize ohlajevalnih krivulj

From the cooling-curve analyses, the latent heat and liquid fraction at characteristic solidification points can be obtained. Knowing these values is important in order to understand the solidification characteristics of the alloy. The latent heat can be calculated by multiplying the accumulative area between the first derivative and the baseline by the specific heat.⁹ The liquid fraction can be obtained by calculating the accumulative area between the first derivative and the baseline from the characteristic solidification points to the solidification end point as a fraction of the total area between these curves.⁸

Figure 7 shows the calculated latent heat and the liquid fractions at the DCP and FICP. The latent heat increased with increasing Mg and Si in the Al-*x*Mg-1Fe-0.5Si and Al-*x*Si-1Fe-1Zn alloys, as shown in **Figure 7a**. These results are different from the thermophysical modeling results of **Figure 3a**, in which the increase of Mg content decreased the latent heat of the Al-*x*Mg-1Fe-0.5Si alloys. This contrasting tendency of the latent heat with increasing Mg content is responsible for the difference in the solidification path between the phase equilibria calculation and the actual non-equilibrium solidification. In any case, it seems that the latent heat did not have a significant effect on the fluidity of these experimental alloys. In the liquid fractions at the DCP and FICP of **Figure 7b**, two interesting findings were obtained. First, in the Al-*x*Mg-1Fe-0.5Si alloys, the liquid fraction was

higher at FICP than at DCP, but this tendency is reversed in the Al- x Si-1Fe-1Zn alloys. Second, in the Al- x Mg-1Fe-0.5Si alloys, the liquid fractions at DCP and FICP increased with increasing Mg content, whereas in the Al- x Si-1Fe-1Zn alloys, the liquid fractions decreased with increasing Si content. The dendrite coherency seriously decreases the fluidity.¹⁹ Therefore, it is likely that in the Al- x Si-1Fe-1Zn alloys, although the crystallization of the plate-like β -AlFeSi phase during solidification has a negative effect on the fluidity of Al alloys¹³ and the amount of the β -AlFeSi phase increased with increasing Si content, as shown in **Figures 6c** and **6d**, its crystallization after DCP had little influence on the fluidity. It was thus concluded that in the Al- x Si-1Fe-1Zn alloys, the increase of the Si content effectively improved the fluidity by increasing the latent heat and lowering the DCP without disturbing the secondary phases, whereas in the Al- x Mg-1Fe-0.5Si alloys the secondary phases could have a negative effect on the fluidity because they crystallized before the dendrite coherency. Paes¹⁴ and Zhang¹⁵ reported that the presence of a Mg₂Si phase increased the viscosity of Al alloys. Considering that the liquid fraction of the Al-1.5Mg-1Fe-0.5Si alloy was approximately 50 % at FICP, the increase of the melt viscosity could be regarded as the most important factor in terms of decreasing the fluidity. Therefore, it was concluded that in the Al- x Mg-1Fe-0.5Si alloys, the increase of Mg content significantly deteriorated the fluidity by increasing the viscosity and increasing the DCP, in spite of the increase in the latent heat.

4 CONCLUSIONS

For the development of an aluminum alloy that combines a high thermal conductivity with a good castability and anodizability, the low-Si-containing aluminum alloys Al-(0.5–1.5)Mg-1Fe-0.5Si and Al-(1.0–1.5)Si-1Fe-1Zn were investigated. The obtained results are as follows:

1. The developed aluminum alloys exhibited a thermal conductivity of 170–190 % level (160–180 W/(m K)), a fluidity of 60–85 % level, and an equal or higher ultimate tensile strength compared to those of the ADC12 alloy.
2. In each developed alloy system, the thermal conductivity decreased and the strength increased with increasing amounts of Mg and Si, the major alloying elements. The fluidity exhibited an inverse relationship with the Mg content and a direct relationship with the Si content.
3. The contradictory fluidity variation behavior in the two alloy systems with the compositions of Mg and Si was caused by the opposing tendencies of DCP and FICP and the relatively different occurring sequences of DCP and FICP.
4. In the experimental aluminum alloys with a low Si content, the prevailing Fe-containing intermetallic compound and the solidification path were observed to be mainly dependent on the Si segregation beha-

avior and the Mg alloying level, rather than on the initial Si/Fe alloying ratio.

5. It was found that the Al-Mg-Fe-Si-based aluminum alloys that show a higher strength and good fluidity in channels greater than 2 mm in diameter are potential materials for general cast heat-dissipating components, and that the Al-Si-Fe-Zn-based aluminum alloys that possess a lower surface energy are potential materials for thin-wall cast heat-dissipating components.

5 REFERENCES

- ¹ G. P. Reddy, N. Gupta, Material selection for microelectronic heat sinks, *Materials and Design*, 31 (2010), 113–117
- ² K. P. Keller, Efficiency and cost tradeoffs between aluminum and zinc die cast heatsinks, *Proc. of Inter. Electronic Packaging Conf.*, 1997
- ³ K. P. Keller, Low cost, high performance, high volume heatsinks, *Proc. of 1998 IEMT-Europe Symposium*, Berlin, 1998
- ⁴ S. Ferlini, A. Morri, E. Ferri, M. Merlin, G. Giacomozzi, Effect of silicon particles and roughness on the surface treatments of cast aluminum alloys, *Proc. of the 3rd Iner. Conf. on High Tech Die Casting*, Vicenza, 2006
- ⁵ J. E. Hatch, *Aluminum-Properties and Physical Metallurgy*, 10th ed., ASM, Ohio 2005, 210
- ⁶ W. F. Gale, T. C. Totemeier, *Smithells Metals Reference Book*, 8th ed., ASM, Oxford 2004, 8-2
- ⁷ A. T. Dinsdale, P. N. Quedsted, The viscosity of aluminum and its alloys-A review of data and models, *Journal of Materials Science*, 39 (2004), 7221–7228
- ⁸ S. Farahany, H. R. B. Rada, M. H. Idris, M. R. A. Kadir, A. F. Lotfabadi, A. Ourdjini, In-situ thermal analysis and macroscopical characterization of Mg- x Ca and Mg-0.5Ca- x Zn alloy systems, *Thermochimica Acta*, 527 (2012), 180–189
- ⁹ I. U. Haq, J. S. Shin, Z. H. Lee, Computer-Aided Cooling Curve Analysis of A356 Aluminum Alloy, *Met. & Mat. Inter.*, 10 (2004), 89–96
- ¹⁰ P. Bastien, J. C. Armbruster, P. Azov, Flowability and viscosity, *AFS Trans.*, 70 (1962), 400–409
- ¹¹ Y. Han, C. Ban, S. Guo, X. Liu, Q. Ba, J. Cui, Alignment behavior of primary Al₃Fe phase in Al-Fe alloy under a high magnetic field, *Materials Letters*, 61 (2007), 983–986
- ¹² E. Taghaddos, M. M. Hejazi, R. Taghiabadi, S. G. Shabestari, Effect of iron-intermetallics on the fluidity of 413 aluminum alloy, *Journal of Alloys and Compounds*, 468 (2009), 539–545
- ¹³ A. Darvishi, A. Maleki, M. M. Atabaki, M. Zargami, The mutual effect of iron and manganese on microstructure and mechanical properties of aluminium-silicon alloy, *MJoM*, 16 (2010), 11–24
- ¹⁴ M. Paes, E. J. Zoqui, Semi-solid behavior of new Al-Si-Mg alloys for thixoforming, *Mat. Sci. & Eng.*, A406 (2005), 63–73
- ¹⁵ J. Zhang, Z. Fan, Y. Wang, B. Zhou, Hypereutectic aluminium alloy tubes with graded distribution of Mg Si particles prepared by centrifugal casting, *Materials and Design*, 21 (2000), 149–153
- ¹⁶ M. Rosefort, C. Matthies, H. Buck, H. Koch, *Light Metals 2011*, TMS 2011, 711–715
- ¹⁷ B. Dutta, M. Rettenmayr, Effect of cooling rate on the solidification behaviour of Al-Fe-Si alloys, *Mat. Sci. & Eng.*, A283 (2000), 218–224
- ¹⁸ M. Hosseinifar, D. V. Malakhov, The Sequence of intermetallics formation during the solidification of an Al-Mg-Si alloy containing La, *Met. & Mat. Trans.*, 42A (2011), 825–833
- ¹⁹ S. Nafisi, R. Ghomashchi, Combined grain refining and modification of conventional and rheo-cast A356 Al-Si alloy, *Mat. Char.*, 57 (2006), 371–385